Vis Comput (2012) 28:1039–1048
DOI 10.1007/s00371-012-0731-y

ORIGINAL ARTICLE

Crowd simulation: applying mobile grids to the social force model

Priscila Saboia · Siome Goldenstein

Published online: 30 May 2012

Abstract The social force model (SF) is able to reproduce many emergent phenomena observed in real crowds. Unfortunately, in some situations, such as low density environments, SF may produce counterintuitive results where the trajectories simulated look more like particles than to real people. We modify the SF model through the use of a mobile grid to allow the simulated pedestrians to change the direction of their desired velocity at reasonable times, thus avoiding nearby blocked or crowded areas smoothly. Our experiments focus on qualitative behavior, and verify that our model produces the desired trajectories of the pedestrians, achieving softer and more coherent trajectories when compared to the pure SF model solution. Like SF, our model reproduces the "faster-is-slower" and the arching underlying the clogging effects. Finally, we examine the occupation rates of the space when pedestrians were submitted to narrowed corridors and observe the "edge effect."

Keywords Crowd simulation · Social force model · Mobile grid

1 Introduction

A crowd is as a large group of individuals in the same physical environment, sharing a common purpose, with the possibility of acting differently than when they are by themselves [5].

P. Saboia (✉) · S. Goldenstein
Institute of Computing, University of Campinas, Campinas, SP, Brazil
e-mail: psaboia@ic.unicamp.br

The movement of crowds includes a number of different people, or agents, moving independently in a shared environment, aiming to reach specific destinations. Understanding the movement of crowds is essential to plan and improve public places, not only to facilitate and expedite the movement of citizens, but also to guarantee their safety, especially in conditions of imminent danger when there is need for evacuation.

Behavior patterns in crowds arise from the interactions and influences between individuals and environment. Dynamic aspects of evacuation processes have been characterized through modeling, due to the absence of data from real evacuations. Several computer models have been proposed in this direction. The social force model (SF) [5] is one of them, in which the motion of each pedestrian is a result of both physical and psychological forces.

This model has described successfully phenomena such as the "faster-is-slower" and the arching underlying the clogging effects. Nevertheless, in some low-density scenarios, experiments show that the simulated individuals do not behave as expected, working as irrational particles rather than rational people. For example, in the cited model, it is common to watch many simulated individuals going repeatedly and directly towards columns, rather than finding a way to deviate and safely exit the room. This occurs because the desired direction of a pedestrian's motion always points to the target position, even in the presence of obstacles (or other pedestrians) between its current position and the target position.

Here, we modify the SF model, redesigning the force of desire in order to permit pedestrians to change their desired direction of movement voluntarily, based on their perceptions of other pedestrians and obstacles in their surroundings. We mapped the space around each pedestrian as a mobile grid, (as in [3]) in order to obtain spatial informa-

tion concerning the surroundings and to choose the desire fore direction used in the SF model. In our experiments, we show that the modified model improves the trajectories of the pedestrians, while maintaining its ability to reproduce the "faster-is-slower" and the arching underlying the clogging effects. Furthermore, our experiments demonstrate the emergent phenomenon called "edge effects" that is observed in real crowds according to Still [19].

2 Related work

We can roughly classify the approaches used for crowd simulation into two categories: macroscopic and microscopic models. Macroscopic models describe the dynamic of the density and velocity of the whole crowd. Within this approach, Hughes [9], Huang et al. [8], and Treuille et al. [21], utilize fluid dynamics to describe the density and velocity of the crowd by the means of partial differential equations. Musse et al. [14] propose a model based on trajectories captured automatically from filmed video sequences. These trajectories are grouped into similar classes and an extrapolated velocity field is generated for each class.

Microscopic models describe the speed and position of each agent in a given time. The work of Reynolds [16] is pioneer in this direction where each simulated bird is implemented as an independent actor that navigates according to its local perception of the dynamic environment. Tu and Terzopoulos [22] simulated groups of artificial fishes.

Kapadia et al. [10] propose the use of egocentric affordance fields for obtain the speed and the direction of each pedestrian at each step simulation. Varas et al. [23] and Perez et al. [15] introduce cellular automata models for motion, in which pedestrians are located at nodes of a grid and their coordinates are updated at discrete time intervals. Muramatsu et al. [12], Tajima and Nagatani [20], and Guo and Huang [3] define navigational models by probabilistic and statistic functions based on lattice-gas concepts, a special case of cellular automata.

Lerner et al. [11] present a approach for fitting behaviors to simulated pedestrian crowds. These behaviors go beyond the walk such as talk on cellular, comb hair, move the head left, right, down, and back. Musse and Thalmann [13] proposed a hierarchical crowd organization with groups of different autonomy levels. Goldenstein et al. [1] used nonlinear approach for agent control. Two nonlinear dynamic systems run in parallel, one for the heading direction, and the second for assisting the data fusion of the attractors and repellers. Later, the authors used the low-level system in a hybrid configuration [2] that allowed complex crowd environments and a global solution without agents getting stuck in local minima. Finally, social force models introduced by Helbing et al. [5] describe the motion of each pedestrian as a result of physical and psychological forces. The crowd dynamics is consequence of local interaction between the pedestrians.

There are two types of analysis over the behavior of individuals in a crowd, quantitative and qualitative. Quantitative analysis is when one or more well-defined measurable quantities have their magnitude accurately measured, allowing comparisons and optimization.

As an example of quantitative analysis, Henderson was a pioneer [7] when collected and established distribution functions for the speed and the velocity of individuals in real crowds. A more recent example is the work by Shao and Terzopoulos [17], which measured, collected, and minimized the number of collisions among the individuals of the crowd.

On the other hand, qualitative analysis is when researchers cling to aspects less susceptible to accurate measurement, such as visual patterns that emerge on the crowd, or specific arrangements of the individuals in space. Following this line of study, Helbing and Molnár [4] and Still [19], were concerned to develop computer models able to reproduce crowd-spatial phenomena such as the "edge effects" and arching underlying the clogging effects.

Lately, facing the diversity of models, metrics, and solutions for the analysis of the movement of crowds, Singh et al. [18] realized the importance of standardizing and facilitating the evaluation and the comparison of the different approaches applied to such problem. Thus, they proposed a benchmark suite for evaluating steering behaviors.

In this paper, we focus our analysis in the qualitative aspects of our method.

3 Overview

We modify the social force model (SF) to improve the way pedestrians approach obstacles and other pedestrians; see Fig. 1. To do so, we redesign the force of desire component of the model to let pedestrians voluntarily change their directions of movement, based on their perceptions of the environment.

For each pedestrian, a mobile grid help us find the direction of movement, inspired by Guo and Huang [3]. We divide the area around the pedestrian in n possible directions, each with a different weight.

At each time t of simulation, the direction of the force of desire of a pedestrian is the one with the greatest weight value on its mobile grid.

In the next sections, we describe the SF in more detail, introduce the mobile grids approach for each pedestrian, as well as the assignment of weight values.

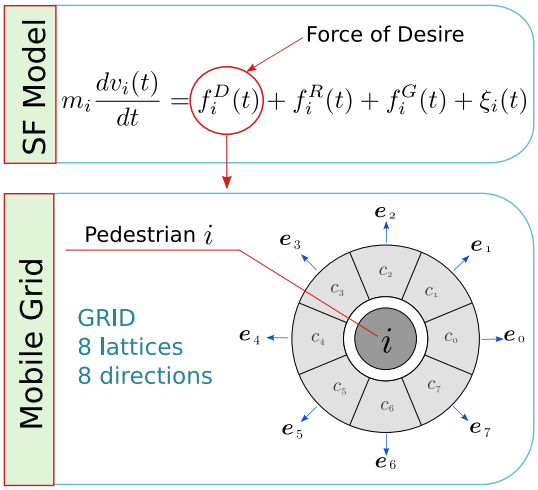

Fig. 1 Illustration of the proposed method. For a pedestrian i in the Social Force Model, the direction of the force of desire $\mathbf{e}$ is the one with the greatest associated weight value C on its mobile grid

4 The social force model

In the social force model (SF) proposed by Helbing et al. [5], each pedestrian's motion takes into account three types of physical and psychological forces: the pedestrian's desire, $\mathbf{f}^D$, the repulsive effect, $\mathbf{f}^R$, and the granular interaction, $\mathbf{f}^G$.

4.1 Effect of a pedestrian's desire

Each pedestrian i of mass m_i wants to reach a target position $\mathbf{r}_i^0$. By doing so, a pedestrian can get a predefined speed $\mathbf{v}_i^0$ (desired velocity) in a certain direction $\mathbf{e}_i$. If $\mathbf{r}_i(t)$ is the present position of a pedestrian i, at time t, its desired direction of motion $\mathbf{e}_i(t)$ is

$$\mathbf{e}_i(t) = \frac{\mathbf{r}_i^0 - \mathbf{r}_i(t)}{|\mathbf{r}_i^0 - \mathbf{r}_i(t)|}, \tag{1}$$

to which the pedestrian tends to adapt its instantaneous velocity v_i within a certain time interval τ. The effect of a pedestrian's desire can be described by the force

$$\mathbf{f}_i^D(t) = m_i \frac{1}{\tau}\big(v_i^0 \mathbf{e}_i(t) - \mathbf{v}_i(t)\big). \tag{2}$$

4.2 Repulsive effect (other pedestrians and obstacles)

Pedestrians try to keep a distance from obstacles and other pedestrians using an interaction force

$$\mathbf{f}_i^R = \sum_{j=1, j\neq i}^{N_p} \mathsf{A}\exp\left(\frac{-x_{ij}}{\mathsf{B}}\right)\mathbf{n}_{ij}, \tag{3}$$

where A represents the intensity of the repulsive force measured in Newtons, and B is a constant value which determines the range of the social interaction, measured in meters, $\mathbf{n}_{ij} = (n_{ij}^1, n_{ij}^2)$ is the two-dimensional unit vector pointing from the entity j (pedestrian or obstacle) to the pedestrian i, and x_{ij} is the distance between pedestrian i and entity j. Note that we model the geometry of pedestrians as circles and the geometry of obstacles, such as walls and columns, as polygons. N_p is the set of the pedestrians and obstacles in the model.

4.3 Granular interaction effect in panicking crowds

There are two additional forces inspired by granular interactions which are essential to the understanding of the emerging behaviors in panicking crowds: a body force $k(-x_{ij})\mathbf{n}_{ij}$, that prevents body compression, and a sliding friction force $\kappa(-x_{ij})\Delta\mathbf{v}_{ji}^t\mathbf{t}_{ij}$ that interferes with the relative tangential motion if pedestrian i comes close to pedestrian j. Here, $\mathbf{t}_{ij} = (-n_{ij}^2, n_{ij}^1)$ means the tangential direction, and $\Delta\mathbf{v}_{ji}^t$ means the tangential velocity difference (k and κ are constants), so

$$\mathbf{f}_i^G = \sum_{j=1, j\neq i}^{N_p} Kg(-x_{ij})n_{ij} + \kappa g(-x_{ij})\Delta\mathbf{v}_{ji}^t\mathbf{t}_{ij}, \tag{4}$$

where the function $g(x)$ is zero if the pedestrians do not touch each other, and x otherwise.

4.4 Motion of a pedestrian

The change in velocity at time t is given by

$$m_i \frac{d\mathbf{v}_i(t)}{dt} = \mathbf{f}_i^D(t) + \mathbf{f}_i^R(t) + \mathbf{f}_i^G(t) + \xi_i(t), \tag{5}$$

where $\xi_i(t)$ represents a fluctuation term that stands for random behavioral variations arising from accidental or deliberate deviations from the optimal strategy of motion. Finally, the change of position $\mathbf{r}_i(t)$ is given by the velocity $\mathbf{v}_i(t) = d\mathbf{r}_i(t)/dt$.

4.5 Mobile grid and force of desire

Here, pedestrians can evaluate and change their directions from time to time. To support the calculation of the new direction, we map the space around each pedestrian as a mobile grid.

Our mobile grid structure is similar to that of Guo and Huang [3], but we do not use probability distribution. Instead, the grid distributes weights to the possible directions and models the occupation of the space around the pedestrians.

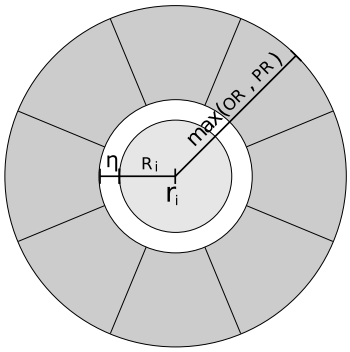

Fig. 2 Mobile grid partitioned into 8 directions around a pedestrian i (*lighter gray circle*)

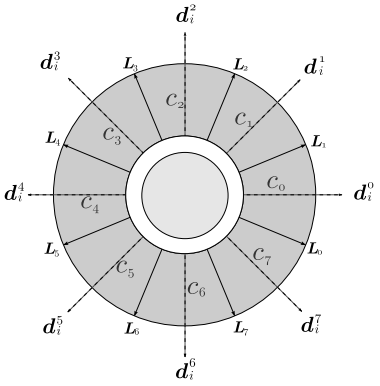

Fig. 3 Lattices and directions of a mobile grid with 8 bins

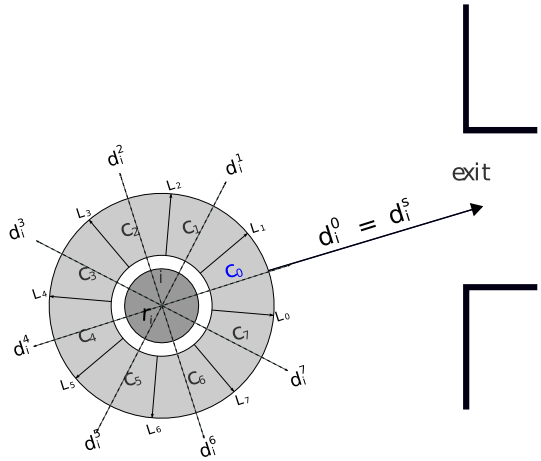

Fig. 4 Grid in the absence of obstacles in the direction of the vector $\mathbf{d}_i^s$

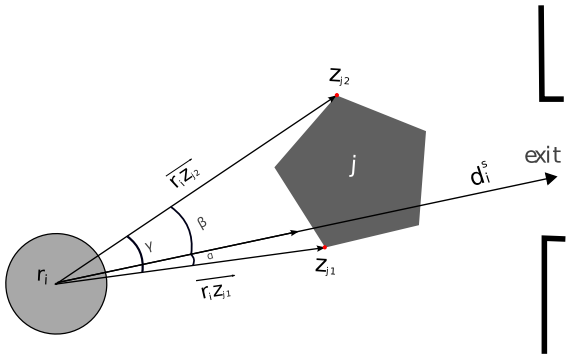

Fig. 5 Endpoints $\mathbf{z}_{j1}$ and $\mathbf{z}_{j2}$ of the object j

5 Mobile grid

Just as in the SF model, each pedestrian i is represented by a circle of radius R_i. The mobile grid is an area formed by an annulus around a pedestrian i, evenly partitioned into n directions, or bins. It is conventional to name as lattice each one of the partitions, denoted by c_k, where $k \in [0, n-1]$.

The annulus is formed by two concentric circles of center $\mathbf{r}_i(t)$, where the inner radius of the circle is given by $R_i + \eta$, and the radius of the external circumference is given by the radius of the pedestrian's greatest neighborhood, i.e., $\max(PR, OR)$, where PR represents the radius of the neighborhood of the pedestrian i in relation to other pedestrians, and OR represents the radius of the neighborhood in relation to obstacles. The constant η represents the minimum distance at which a pedestrian desires to be from other pedestrians and obstacles. Figure 2 shows a pedestrian's current position and an annulus around it.

The lattices are bounded by vectors in the sequence $\mathbf{L}_0, \mathbf{L}_1, \ldots, \mathbf{L}_{n-1}$, as illustrated in Fig. 3. Each lattice c_k has an opening angle $\theta = 360°/n$, a direction defined by the vector $\mathbf{d}_i^k$, and two limiting unit vectors $\mathbf{L}_a$ and $\mathbf{L}_b$, respectively put in a counterclockwise direction, with $a = (i \bmod n)$ and $b = ((i+1) \bmod n)$.

Moreover, lattices are arranged in the counterclockwise direction on the basis of the output vector $\mathbf{d}_i^s$ (obtained in the same way that $\mathbf{e}_i$ in Eq. (1)).

In the absence of obstacles in the direction of the vector $\mathbf{d}_i^s$, the grid is arranged so that the lattice c_0 has its representative vector $\mathbf{d}_i^0 = \mathbf{d}_i^s$, (Fig. 4). Otherwise, the direction of $\mathbf{d}_i^0$ is obtained by taking into account the vector $\mathbf{d}_i^s$ and the endpoints of the object j in relation to the pedestrian i.

Considering the points $\mathbf{z}_{j1}$ and $\mathbf{z}_{j2}$ as endpoints of the object j, they are obtained based on the angle subtended by j to $\mathbf{r}_i(t)$, which is the center of the pedestrian i, as one can see in Fig. 5. Thus, once defined the endpoints and data vectors $\mathbf{r}_i\mathbf{z}_{j1}$ and $\mathbf{r}_i\mathbf{z}_{j2}$, the vector $\mathbf{d}_i^0$ is equal to the vector among those which present the smallest angle with the vector $\mathbf{d}_i^s$ (Fig. 6).

The grid is the mechanism to find the new desired direction of the velocity $\mathbf{e}_i(t)$ in Eq. (2). For that, there is a weight distribution (P_i^k) between its lattices, indicating the likelihood of choosing each one. The direction of the chosen lattice will be the new desired direction of the velocity.

6 Distribution of weights on the grid

For a pedestrian i, the distribution of weights for each lattice k is denoted by P_i^k

$$P_i^k = N\delta_i^k I^k\left(D_i^k + \frac{Access_i^k}{2}\right). \tag{6}$$

The term $Access_i^k$ represents the measure of the accessibility of the lattice c_k to a pedestrian i, i.e., how much obstacles and pedestrians are not obstructing the passage of the pedestrian i through the given lattice k. It is calculated by the lowest value of S_{ij}^k

$$Access_i^k = \min_{j\in\omega_i}\left(S_{ij}^k\right), \tag{7}$$

where the set ω_i represents all the pedestrians and obstacles in the neighborhood of the pedestrian i. The term $S_{i,j}^k$ represents how much the pedestrian i is walking away from j, inside the lattice k. Its value varies in the interval [0, 1], and is calculated by

$$S_{i,j}^k = \begin{cases} 1, & j \text{ doesn't intersect } k, \\ A_{i,j}^k + (1 - A_{i,j}^k)B_{i,j}^k, & \text{otherwise}, \end{cases} \tag{8}$$

where the value of A_{ij}^k represents a percentage of separation between the pedestrian i and the part of the pedestrian (or obstacle) j which has an intersection with the lattice k,

$$A_{i,j}^k = \begin{cases} 0, & \text{if } H_{i,j}^k \le \eta, \\ \frac{H_{i,j}^k - \eta}{\rho - H_{i,j}^k}, & \text{if } \eta < H_{i,j}^k < \rho, \\ 1, & \text{if } H_{i,j}^k \ge \rho, \end{cases} \tag{9}$$

where ρ is related to the radius of the neighborhood of the pedestrian i, and j is a neighbor pedestrian. ρ has the same value of the constant PR. On the other hand, being j a neighbor obstacle, ρ has the same value of the constant OR. The constants η and ρ determine the inferior and superior quota, respectively, for the value of $H_{i,j}^k$, which, in turn, represents a measure of the distance between the pedestrian i and the piece of j inside the lattice c_k. It is illustrated by Fig. 7.

In the Eq. (8), the term $B_{i,j}^k$ represents the percentage of θ, which is the angular opening of the lattice c_k that is not occupied by the piece of the pedestrian j that lies on the lattice c_k,

$$B_{i,j}^k = \frac{\alpha_{i,j}^k}{\theta}, \tag{10}$$

where the term $\alpha_{i,j}^k$ is an angular value in the interval $[0, \theta]$ and represents a free angular opening of the lattice c_k. In the case of nonoccurrence of any endpoint of j inside the region of the lattice c_k, $\alpha_{i,j}^k$ must assume a null value, as illustrated in Fig. 8(a). This happens when j occupies c_k so that any angular opening is free, as in Fig. 8(b). The term D_i^k (still referring to Eq. (6)) represents the strength that makes a pedestrian walk towards its target according to the vector d_i^0

$$D_i^k = D\frac{(\cos(\theta_{k,0}) + 1)^2}{4}, \tag{11}$$

where the drift D, of which value is between 0 and 1, represents the strength drifting in the direction d_i^0 from the pedestrian's current position to exit. $\theta_{k,0}$ is the angle between the unit vector in direction d_i^k and the unit vector in direction d_i^0. Figure 9 shows the angle $\theta_{2,0}$ related to lattice c_2. For a given lattice, its value is proportional to its likelihood to the exit direction d_i^0. This guarantees that pedestrians have lower preference to take directions opposite to the exit.

The term N is a normalization factor responsible for ensuring that $\sum_d P_i^k = 1$, and δ_i^k models people's preference

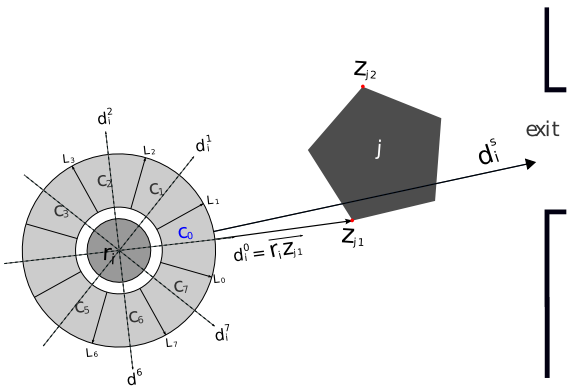

Fig. 6 Grid in the presence of an obstacle j in the direction of the vector $\mathbf{d}_i^s$

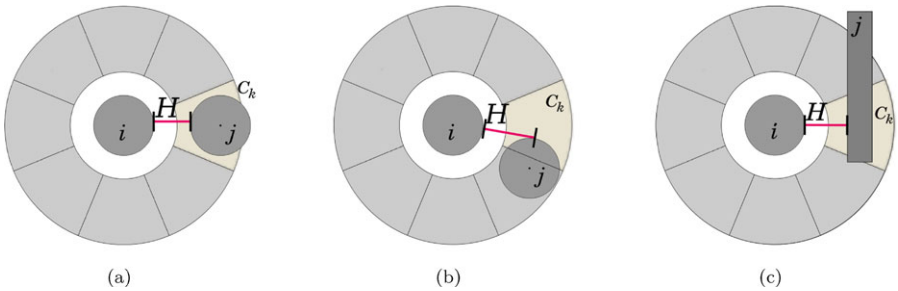

Fig. 7 Distance $H_{i,j}^k$ used in the calculation of $A_{i,j}^k$ in three possible situations. (**a**) Central point of j is at the lattice c_k. (**b**) There is an endpoint of j at the lattice c_k. (**c**) Neither the central point of j nor its endpoints are at c_k

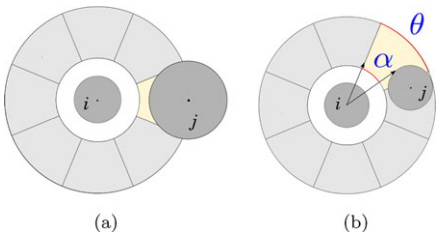

Fig. 8 Free angular opening $\alpha_{i,j}^k$ of the lattice c_k for a pedestrian i and a neighbor j. (**a**) Neither endpoint of j is inside the region of the lattice c_k ($\alpha_{i,j}^k = 0$). (**b**) Pedestrian j does not occupy all the lattice c_k

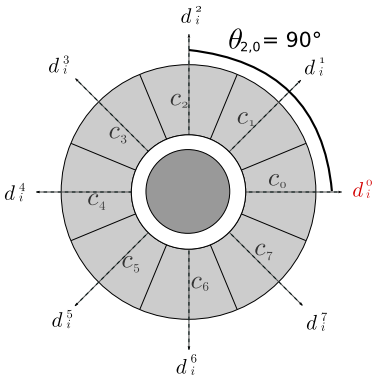

Fig. 9 For a grid with 8 partitions, there is the angle $\theta_{2,0}$ related to lattice c_2

for directions where others are not too close, in low and medium densities. It takes values 0 or 1,

$$\delta_i^k = \begin{cases} 0, & \text{if } Access_i^k = 0, \\ 1, & \text{if } Access_i^k \neq 0. \end{cases} \tag{12}$$

The term I^k is bigger than 1 when the chosen direction in the previous step is related to the lattice k, otherwise its value is 1. This term represents the preference of a pedestrian for maintaining the chosen direction of its previous movement.

7 The desired direction of motion

The sum of access terms for a pedestrian i sets a "rate of occupancy" of the space around it. If this sum is above a threshold λ, it indicates that there is space for the pedestrian to go around other pedestrians (conditions of low and medium densities). Otherwise, the pedestrian will keep the direction of motion similar to the SF model (conditions of high densities).

After calculating the weights of each lattice of the grid, if the sum of the factors of access is above the threshold λ, the desired direction e_i of the pedestrian i will be the direction of the lattice that received the greatest weight, otherwise the direction will be d_i^0.

8 Experiments

We conducted experiments to verify that the modified model produces changes in the trajectories of the pedestrians, while the crowd maintains qualitative properties such as the ability to reproduce the "faster-is-slower" effect, the arching underlying the clogging effects, and the "edge effect."

In all experiments, we model each pedestrian as a circle of which radius followed a Gaussian distribution with mean 0.6 m and standard deviation 0.1 m. For the beginning of each simulation, we distributed all pedestrians randomly in the simulated space.

In the first two experiments, we propose a scenario of people in danger while attempting to leave a room with only one exit door. In the third experiment, we propose a scenario where people are trying to pass a narrow corridor in an ordinary situation (i.e., with no panicking elements).

For all simulations, each pedestrian was set up as follows: $\tau = 0.5$ s, $A = 2 \cdot 10^3$ N (Newtons), $B = 0.08$ m, $K = 1.2 \cdot 10^5$ kg/s^2 and $\kappa = 2.4 \cdot 10^5$ kg/m/s. Such values were properly applied to Eq. (2), Eq. (3), and Eq. (4).

For each pedestrian the grid had eight (8) lattices, the radius *PR* of the neighborhood related to other pedestrians was 0.8 m, the radius *OR* of the neighborhood related to obstacles was 4.0 m, η was 0.4 m, the threshold λ was 1.25, the inertia I^k (to maintain the previous direction) was 1.2, and the drift D was 1.0.

8.1 Evacuation of a room with an obstacle

In this experiment, we wanted to verify whether there was any improvement on the trajectories of the pedestrians compared to the original SF model. To do so, we presented sixty (60) pedestrians to a single-door room, of which dimensions were 15 m × 15 m, with a 1.2 m-wide door and, the most important, a column with 2 m of radius, right in front of the exit. The pedestrians' desired velocities were set as $v^0 = 5$ m/s.

The trajectories resulting from the simulation of this scenario are shown as black lines in Fig. 10. Figure 10(a) shows results for the original model, and 10(b) shows results for our model.

8.2 Evacuation of a room versus desired velocity

In this experiment, we perform a quantitative test to our model to determine whether it maintains the "faster-is-slower" effect [5].

We execute several simulations using one hundred and fifty (150) pedestrians to the same single-door simulated room. From one simulation to the other, we change only the desired velocities of the pedestrians, and then collect the average evacuation times. We can then verify whether the

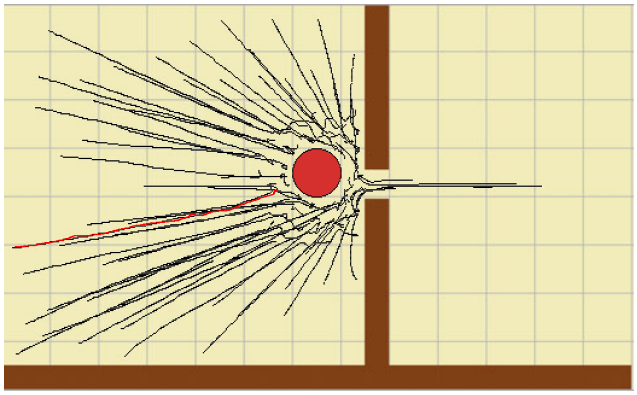

(a) SF model

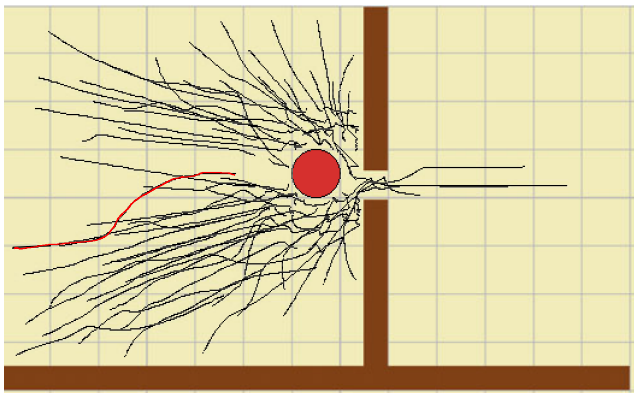

(b) Our model

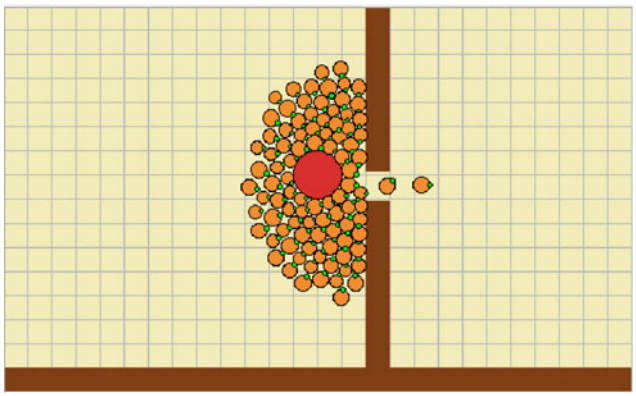

(c) Pedestrians are represented by orange circles

Fig. 10 (**a**) and (**b**) Trajectories of 60 pedestrians in the first experiment. (**c**) Screenshot of the first experiment with the modified SF model 5.38 s after initialization

time for all pedestrians to leave the room decreases when the desired velocities are increased, just as it occurs in the SF model.

We use the same room similar of the first experiment, except for the column. We place 150 randomly distributed pedestrians with the same desired velocity, and each simulation had the following values for the desired velocities v^0: 0.8, 1.0, 1.5, 1.75, 2.0, 2.25, 2.5, 3.0, 3.5, 4.0, 5.0, 6.0, and 7.0.

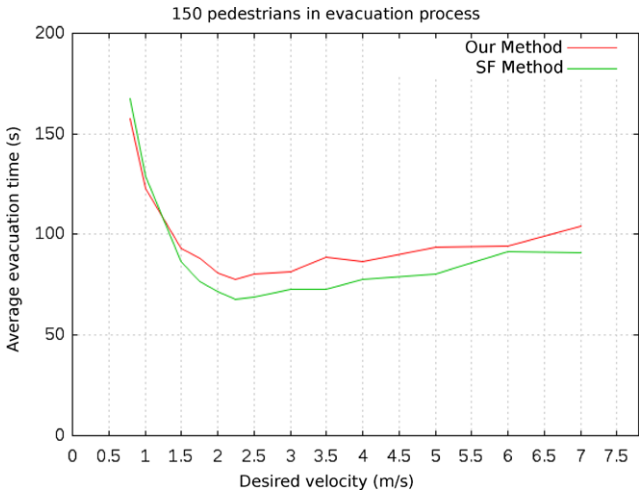

Fig. 11 Evacuation times of the pedestrians for various desired velocities v^0

Figure 11 shows the relation between the average evacuation time and the desired velocity obtained from simulations with the original and the modified SF models.

8.3 Narrowed corridor

In this experiment, we perform a qualitative test on our model to determine whether it reproduces the "edge effects" emergent phenomena, observed in real crowds.

As described by Still [19], the "edge effects" occurs in narrowed corridors, with a bottleneck formation. When people go through the corridor, right after the end of the bottleneck the crowd maintains itself constricted as if the constricting formation was still there.

To reproduce such situation, we create a scenario with a 40 m long narrowed corridor, of which varying widths were 12 m, 8 m, and 12 m (see Fig. 12(a) for details). People accessed the corridor from its left side at a 20 pedestrians/s rate. After 30 s of simulation, at least six hundred (600) people entered the space with the same desired velocity of 1.35 m/s (see Fig. 12(b)).

We use dynamic density and average speed based maps to visualize the "edge effects" phenomena with a color code (see Fig. 13) similar to Still's [19].

Figures 14(a) and 14(b) display the average speed and dynamic density based maps, respectively, at 30 s of simulation. For the average speed, the smallest and largest values were 0 and 2.4 m/s, respectively. For the dynamic density, its smallest and largest collected values were 0 and 4 pedestrians/m^2, respectively.

9 Results and discussion

According to the results from the first experiment, in Fig. 10, our model produces significant changes in the trajecto-

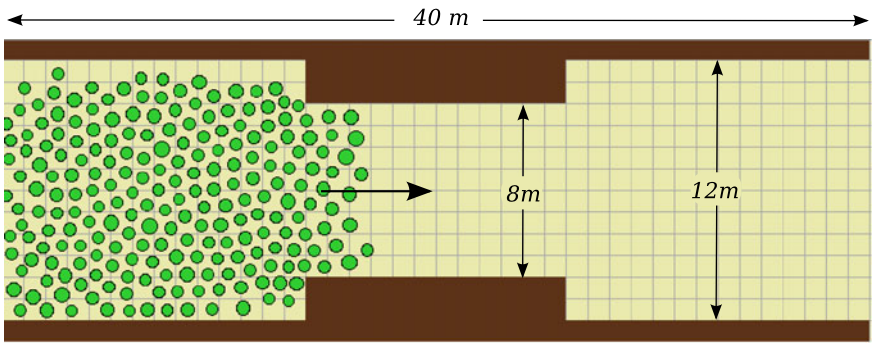

(a) 10 seconds after initialization

(b) 30 seconds after initialization

Fig. 12 Scenario with a narrowed corridor verifies the existence of the "edge effect"

(a) Speed scale. Green (slow) - Red (Fast)

(b) Density scale. Blue (low) - Red (high)

Fig. 13 Color scale of the maps. (**a**) the *green-to-red* scale for speed and (**b**) the *blue-to-red* scale for density

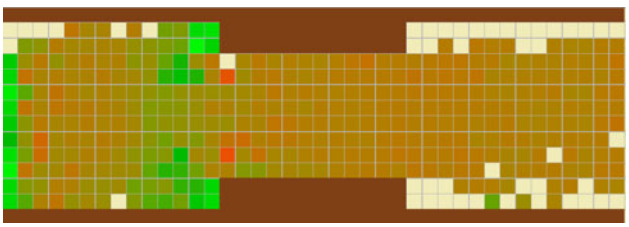

(a) Speed Average Map

(b) Dynamic Density Map

Fig. 14 Speed average and dynamic density maps 30 seconds after initialization

ries of the pedestrians when compared to the SF model. The SF produces trajectories similar to straight lines, as pedestrians neither deviate from the column nor from other pedestrians, even when there are possibilities to circumvent them.

To illustrate this situation, the red lines in Fig. 10 represent the trajectories of a same pedestrian, simulated in both models. The red line produced by the original model is straight, as shown in Fig. 10(a). On the other hand, the line produced by our model is curved, as in Fig. 10(b). This happened due to the changes applied to the pedestrian's desired directions. According to Fig. 10(c), we can observe the appearance of arching near the exit, even for a simulation with the modified model. This shows that our model is also able to reproduce the arching underlying the clogging effect.

In the second experiment, Fig. 11, we observe the "Faster-is-slower" effect. For values of v^0 lower than 2.25 m/s, the time it takes for 150 pedestrians to leave the room decreases, in both models, with an increasing v^0. On the other hand, for $v^0 > 2.25$ m/s, the time it takes for them to leave the room increases.

This phenomenon is related to clogging near the exit; the pedestrians trying to move faster cause a smaller average speed of leaving and, consequently, slower evacuation. Although the evacuation times, for the models, have been slightly different, the curves exhibit the same behavior, i.e. they have the same inflection point ($v^0 = 2.25$ m/s). This shows that our model maintains the expected "faster-is-slower" effect.

In the last experiment, Fig. 12, we show that the geometry of the space directly affects the local average speed and the local dynamic density of the crowd. When moving to

a bottleneck formation, the local dynamic density increases immediately before the constricted area and the local average speed decreases. The space immediately after the end of the constricted area is not entirely occupied. This shows that our model reproduces the expected "edge effect."

10 Conclusions and future work

Simple local models are computationally efficient for simulations, scale well, and are easily to parallelize. They are a good solution for crowd simulation, as long as the desired crowd behaviors emerge from the combination of these small mindless agents.

We used a mobile grid to improve how pedestrians approach obstacles and other pedestrians in the SF model. Pedestrians evaluate and change their directions from time to time.

We focused on the analysis of the qualitative behaviors of our methods, and our results show that our model improved the trajectories of the pedestrians without losing the ability to reproduce the "faster-is-slower" and the arching underlying the clogging effects. We also show in experiments the effect of a narrowed corridor in the trajectories, where the emergent patterns before and after bottleneck formations occurred as expected [19].

Just as the original SF model, our model does not deal with collision avoidance explicitly. Our model is a microscopic agent control mechanism and has no global way to enforce that two pedestrians cannot occupy the same space, which can happen with a poor configuration of parameter values. This is a common drawback of force-based methods for agent control. Also, for complex environments with maze-like structures, it is necessary to add extra steps to estimate the direction of desire, such as harmonic functions. Hybrid methods [2] try to remediate these drawbacks with the combination and interaction of multiple local and global modules.

In the future, we intend to study our model in scenarios with counterflow [12]. We also plan to investigate if our model is able to simulate the effects of "stop-and-go waves," and the real crowd phenomena called "crowd turbulence" [6].

Acknowledgements We would like to thank CNPq, CAPES, and FAPESP for the financial support. We also express our gratitude to Dirk Helbing, Illés Farkas, and Tamás Vicsek for kindly providing us with their source code.

References

1. Goldenstein, S., Large, E., Metaxas, D.: Non-linear dynamical system approach to behavior modeling. Vis. Comput. **15**(7), 349–364 (1999)
2. Goldenstein, S., Karavelas, M., Metaxas, D., Guibas, L., Aaron, E., Goswami, A.: Scalable nonlinear dynamical systems for agent steering and crowd simulation. Comput. Graph. **25**(6), 983–998 (2001)
3. Guo, R., Huang, H.: A mobile lattice gas model for simulating pedestrian evacuation. Physica A, Stat. Mech. Appl. **387**(2–3), 580–586 (2008)
4. Helbing, D., Molnár, P.: Social force model for pedestrian dynamics. Phys. Rev. E, Stat. Phys. Plasmas Fluids Relat. Interdiscip. Topics **51**(5), 4282–4286 (1995)
5. Helbing, D., Farkas, I., Vicsek, T.: Simulating dynamical features of escape panic. Nature **407**(6803), 487–490 (2000)
6. Helbing, D., Johansson, A., Al-Abideen, H.: The dynamics of crowd disasters: An empirical study. Phys. Rev. E, Stat. Nonlin. Soft Matter Phys. **75**(4) (2007)
7. Henderson, L.F.: The statistics of crowd fluids. Nature **229**(5284), 381–383 (1971)
8. Huang, L., Wong, S.C., Zhang, M., Shu, C., Lam, W.H.K.: Revisiting Hughes' dynamic continuum model for pedestrian flow and the development of an efficient solution algorithm. Transp. Res., Part B, Methodol. **43**(1), 127–141 (2009)
9. Hughes, R.L.: A continuum theory for the flow of pedestrians. Transp. Res., Part B, Methodol. **36**(6), 507–535 (2002)
10. Kapadia, M., Singh, S., Hewlett, W., Faloutsos, P.: Egocentric affordance fields in pedestrian steering. In: Proceedings of the 2009 Symposium on Interactive 3D Graphics and Games, pp. 215–223 (2009)
11. Lerner, A., Fitusi, E., Chrysanthou, Y., Cohen-Or, D.: Fitting behaviors to pedestrian simulations. In: Eurographics Symposium on Computer Animation, pp. 199–208 (2009)
12. Muramatsu, M., Irie, T., Nagatani, T.: Jamming transition in pedestrian counter flow. Physica A, Stat. Theor. Phys. **267**(3–4), 487–498 (1999)
13. Musse, S., Thalmann, D.: Hierarchical model for real time simulation of virtual human crowds. IEEE Trans. Vis. Comput. Graph. **7**, 152–164 (2001)
14. Musse, S., Jung, C., Jacques, J. Jr., Braun, A.: Using computer vision to simulate the motion of virtual agents: Research articles. Comput. Animat. Virtual Worlds **18**(2), 83–93 (2007)
15. Perez, G.J., Tapang, G., Lim, M., Saloma, C.: Streaming, disruptive interference and power-law behavior in the exit dynamics of confined pedestrians. Physica A, Stat. Mech. Appl. **312**(3–4), 609–618 (2002)
16. Reynolds, C.: Flocks, herds and schools: A distributed behavioral model. SIGGRAPH **21**(4), 25–34 (1987)
17. Shao, W., Terzopoulos, D.: Autonomous pedestrians. In: Eurographics Symposium on Computer Animation, pp. 19–28 (2005)
18. Singh, S., Kapadia, M., Faloutsos, P., Reinman, G.: Steerbench: A benchmark suite for evaluating steering behaviors. Comput. Animat. Virtual Worlds **20**(5–6), 533–548 (2009)
19. Still, G.: Crowd dynamics. Ph.D. thesis, Mathematics Department, Warwick University (2000)
20. Tajima, Y., Nagatani, T.: Scaling behavior of crowd flow outside a hall. Physica A, Stat. Mech. Appl. **292**(1–4), 545–554 (2001)
21. Treuille, A., Cooper, S., Popović, Z.: Continuum crowds. In: SIGGRAPH, pp. 1160–1168 (2006)
22. Tu, X., Terzopoulos, D.: Artificial fishes: Physics, locomotion, perception, behavior. In: SIGGRAPH, pp. 43–50 (1994)
23. Varas, A., Cornejo, M., Mainemer, D., Toledo, B., Rogan, J., Munoz, V., Valdivia, J.: Cellular automaton model for evacuation process with obstacles. Physica A, Stat. Mech. Appl. **382**(2), 631–642 (2007)

Priscila Saboia was born in Belem, Brazil. She received the B.Sc. degree in Computer Science from the Federal University of Para (UFPA), Brazil, in 2006. After a year acting in the software development market as a systems analyst and as a software test engineer, she decided to move to Campinas, Brazil, in order to join the University of Campinas (UNICAMP), as a M.Sc. candidate. By doing research in the field of crowd simulation, the M.Sc. degree was obtained in 2010, from the Computer Institute at Unicamp (IC-UNICAMP). In the same year, she was accepted for Ph.D. studies at the same institute, this time doing research about shredded document reconstruction, in the field of computer forensics.

Siome Goldenstein is an Associate Professor at the Institute of Computing, University of Campinas, Unicamp, Brazil and a senior IEEE member. He received a Ph.D. in Computer and Information Science from the University of Pennsylvania in 2002, a M.Sc. in Computer Science from Pontificia Universidade Catolica do Rio de Janeiro in 1997, and an Electronic Engineering degree from the Federal University of Rio de Janeiro in 1995. His interests lie in computer vision, computer graphics, computer forensics, and machine learning.

He is an Area Editor of two journals, Computer Vision and Image Understanding (CVIU) and Graphicsl Models (GMOD), has been in the program committee of multiple conferences and workshops, was the local organizer of the 2007 IEEE Intl. Conference on Computer Vision in Brazil, and was co-chair of the 2007 IEEE Workshop on Computer Vision Applications for Developing Regions, and co-chair of the 2008 IEEE Workitorial of vision of the unseen.